Dedifferentiation and aberrations of the endolysosomal compartment characterize the early stage of nephropathic cystinosis

Claudia Raggi[1],[†], Alessandro Luciani[2],[†], Nathalie Nevo[3],[5], Corinne Antignac[3],[4],[5], Sara Terryn[1] and Olivier Devuyst[1],[2],[*]

[1]Division of Nephrology, Université catholique de Louvain, Brussels, Belgium, [2]Institute of Physiology, Zurich Center for Integrative Human Physiology, University of Zurich, Zurich, Switzerland, [3]Inserm U983, Paris, France, [4]Department of Genetics, Centre de Référence MARHEA, Hôpital Necker-Enfants Malades, Paris, France and [5]Sorbonne Paris-Cité, Université Paris Descartes, Imagine Institute, Paris, France

Nephropathic cystinosis, a lysosomal storage disease caused by mutations in the *CTNS* gene encoding the lysosomal cystine transporter cystinosin, is characterized by generalized proximal tubule (PT) dysfunction that progresses, if untreated, to end-stage renal disease. The pathogenesis of defective PT cellular transport in nephropathic cystinosis remains unclear. We characterized a recently generated line of C57BL/6 *Ctns* mice and analyzed endocytic uptake, lysosome function, and dedifferentiation and proliferation markers using primary cultures of PT epithelial cells derived from *Ctns*$^{-/-}$ and *Ctns*$^{+/+}$ littermates. Metabolic studies revealed that *Ctns*$^{-/-}$ mice show a progressive PT dysfunction characterized by low-molecular-weight (LMW) proteinuria, glucosuria and phosphaturia, before structural damage and in the absence of renal failure. These changes are related to decreased expression of the multi-ligand receptors megalin and cubilin and to increased dedifferentiation (ZONAB transcription factor) and proliferation (PCNA and Cyclin D1) rates. Studies on PT cells derived from *Ctns*$^{-/-}$ kidneys confirmed cystine overload, with accumulation of enlarged, dysfunctional lysosomes and reduced expression of endocytic receptors reflected by decreased uptake of specific ligands. These changes were related to a loss of integrity of tight junctions with a nuclear translocation of ZONAB and increased proliferation, as observed in *Ctns*$^{-/-}$ kidneys. These data reveal that the absence of cystinosin in PT cells triggers aberrations of the endolysosomal compartment, transport defects and an abnormal transcription program in the early stage of nephropathic cystinosis. Insights into the early manifestations of cystinosis may offer new targets for intervention, before irreversible renal damage.

INTRODUCTION

The proximal tubules (PTs) of the kidney reabsorb the bulk of filtered solutes and water, through polarized transport systems which reflect terminal differentiation of epithelial cells. Global dysfunction of these transport processes, which is referred to as renal Fanconi syndrome, leads to the excessive urinary loss of solutes (1). In turn, solute losses may cause dehydration and electrolyte imbalance, rickets, muscular weakness, growth retardation and progressive renal failure. Cystinosis is the most frequent form of congenital renal Fanconi syndrome in children (2). The disease is caused by autosomal recessive mutations in the *CTNS* gene that encodes the lysosomal transporter cystinosin (3,4). Loss of cystinosin function results in the accumulation of cystine inside lysosomes and formation of cystine crystals in multiple organs including the kidney. Nephropathic cystinosis (NC), the most severe and frequent form of cystinosis, is characterized by a progressive dysfunction of PT cells that appears by 6–12 months of age. In the absence of treatment with cysteamine, end-stage renal disease is reached around 10 years of age (2).

*To whom correspondence should be addressed at: Institute of Physiology, ZIHP, University of Zurich, Zurich, Switzerland. Tel: +41 0446355082; Fax: +41 0446356814; Email: olivier.devuyst@uzh.ch
†The authors wish it to be known that, in their opinion, the first 2 authors should be regarded as joint First Authors.

The pathogenesis of defective PT transport in NC remains unclear (5). Depletion of intracellular ATP, abnormalities in cellular glutathione levels affecting mitochondrial function and redox state, increased apoptosis, as well as autophagy and mitophagy, have been described in various model systems (5–7). Although these events may coexist at various phases of cell damage, their direct impact on the early defects in transport causing renal Fanconi syndrome is not established. Similarly, the involvement of the multi-ligand receptors megalin and cubilin in the pathogenesis of cystinosis remains unclear. Studies on human biopsy material revealed that the receptors were normally expressed in PT cells (8). Albumin uptake was not affected in clonal cells derived from the urine of cystinotic patients (6), suggesting that the mechanism of low-molecular-weight (LMW) proteinuria may be different in NC than other types of PT dysfunction (5). Information on time course and relative importance of tubular transport defects before onset of renal failure in NC is also lacking, and the link between such defective transport processes, residual cystinosin activity and lysosomal cystine accumulation remains uncertain. Furthermore, treatment with cysteamine, which depletes lysosomal cystine content, does not improve PT dysfunction even when started early in life (2,9).

The difficulty to address mechanisms of PT dysfunction in NC is explained at least in part by limitations of the cellular and animal models used thus far (5). Data obtained either on animal models with incomplete phenotype, on non-renal or non-epithelial cell types, or on clones of transformed cells isolated from urine are difficult to analyze as these cell types may lack essential functions of native PT cells. Renal biopsy material, usually obtained in case of complications or at an advanced disease stage, is of limited value. Until recently, no mouse model mimicking the renal Fanconi syndrome and renal disease associated with cystinosis was available. The first *Ctns*-null mouse model, obtained on a mixed 129/Sv × C57BL/6 genetic background, showed an accumulation of cystine in the kidney and all organs tested, but failed to recapitulate the generalized PT dysfunction that is present in NC patients. Recently, a congenic C57BL/6 *Ctns* line showed accumulation of cystin in the kidney, with signs of tubulopathy, severe histological lesions and chronic renal failure from 10 to 18 months of age (10). We have now used this *Ctns* mouse model to investigate the mechanisms underlying specific transport defects in cystinosis, based on *in vivo*, *ex vivo* and *in vitro* methods. Our results reveal that the absence of cystinosin in PT cells triggers an early chain of events leading to endolysosomal dysfunction, transport defects and dedifferentiation appearing before structural damage and renal failure.

RESULTS

Ctns mice: progression of PT dysfunction

We first used the $Ctns^{-/-}$ mice to characterize the time course and progression of the renal phenotype before the onset of renal failure (Fig. 1, Table 1). When compared with wild-type littermates, $Ctns^{-/-}$ mice showed growth retardation and progressive manifestations of renal Fanconi syndrome, including LMW proteinuria from the age of 12 weeks, followed by polyuria, phosphaturia and glucosuria from 18 weeks. Generalized PT dysfunction was observed at 24 weeks, with inappropriate loss of megalin and cubilin ligands, including vitamin D-binding

protein (DBP), transferring (TF) and procathepsin B, *in the absence* of renal failure (evidenced by similar levels of creatinine clearance and BUN) (Fig. 1A and B; Table 1).

Typical features of nephropathic cystinosis were observed in the $Ctns^{-/-}$ kidneys at this stage: (i) focal atrophy of juxtaglomerular PTs ('swan neck' lesions), restricted to ~5% of the nephrons whereas the renal parenchyma was looking strictly normal (Fig. 1C); and (ii) lysosomal accumulation of cystine crystals in PT cells, as shown by electronic microscopy (Fig. 1C) and cystine assay in kidney cortex (Fig. 1D). As expected, signs of renal failure were detected in *Ctns* mice aged >30 weeks, with increased plasma levels of creatinine and BUN (data no shown).

Abnormal expression of transporters and receptors in $Ctns^{-/-}$ kidneys

Having established the time course of renal Fanconi syndrome in this model, we investigated the expression of transporters and receptors in $Ctns^{-/-}$ kidneys, focusing at 24 weeks of age when PT dysfunction is observed while renal tissue is preserved. These studies revealed that the urinary loss of solutes is associated with decreased expression of specific transporters (including NaPi-IIa and SGLT2) and receptors (megalin/cubilin) in $Ctns^{-/-}$ kidneys, at the mRNA and protein level (Fig. 2A–C). The decreased expression was selective, as other components of PT cells such as the water channel AQP1, the endocytic catalyst Rab5a and the brush border component CD13 (aminopeptidase N) were unaffected (Fig. 2A and B). These data reveal that the early phase of cystinosis is characterized by a specific transport defect *in vivo*, caused by the loss of peculiar receptors and transporters in PT cells.

Defective endocytosis and lysosomal function in PT cells derived from $Ctns^{-/-}$ kidneys

In order to confirm the cell specificity of the endocytic defect observed *in vivo*, we developed primary cultures of PT cells from microdissected PT segments of $Ctns^{-/-}$ mice aged 20 weeks (Fig. 3). It has been shown previously that, when grown on permeable supports, these primary cultured cells preserve their differentiation and polarized transport processes (11). Our functional studies showed that primary cultured PT cells obtained from $Ctns^{-/-}$ kidneys show defective endocytosis as evidenced by an ~70% reduction in albumin uptake when compared with $Ctns^{+/+}$ cells (23 ± 5.0 versus 75 ± 7.1 ng/μg protein.15 min, $n = 5$ pairs, $P < 0.0005$) (Fig. 3A and B). These changes were associated with a decreased expression of megalin and cubilin receptors, as well as of the apical transporters NaPi-IIa and SGLT2 (Fig. 3C–E).

Since nephropathic cystinosis is characterized by lysosomal dysfunction *in vivo*, we next investigated whether an impairment of lysosomal function could be associated with defective endocytosis in PT cells derived from 20-week-old *Ctns* mice. When compared with $Ctns^{+/+}$ control cells, the $Ctns^{-/-}$ cells showed a strong intracellular accumulation of cystine (Fig. 4A), as well as the concentration of all lysosomal-related vesicles into fewer and larger lysosomes that expressed late endosomal/lysosomal markers lysosome-associated membrane protein 1 (LAMP1) or LAMP2 (Fig. 4B). Similar results were obtained using cathepsin
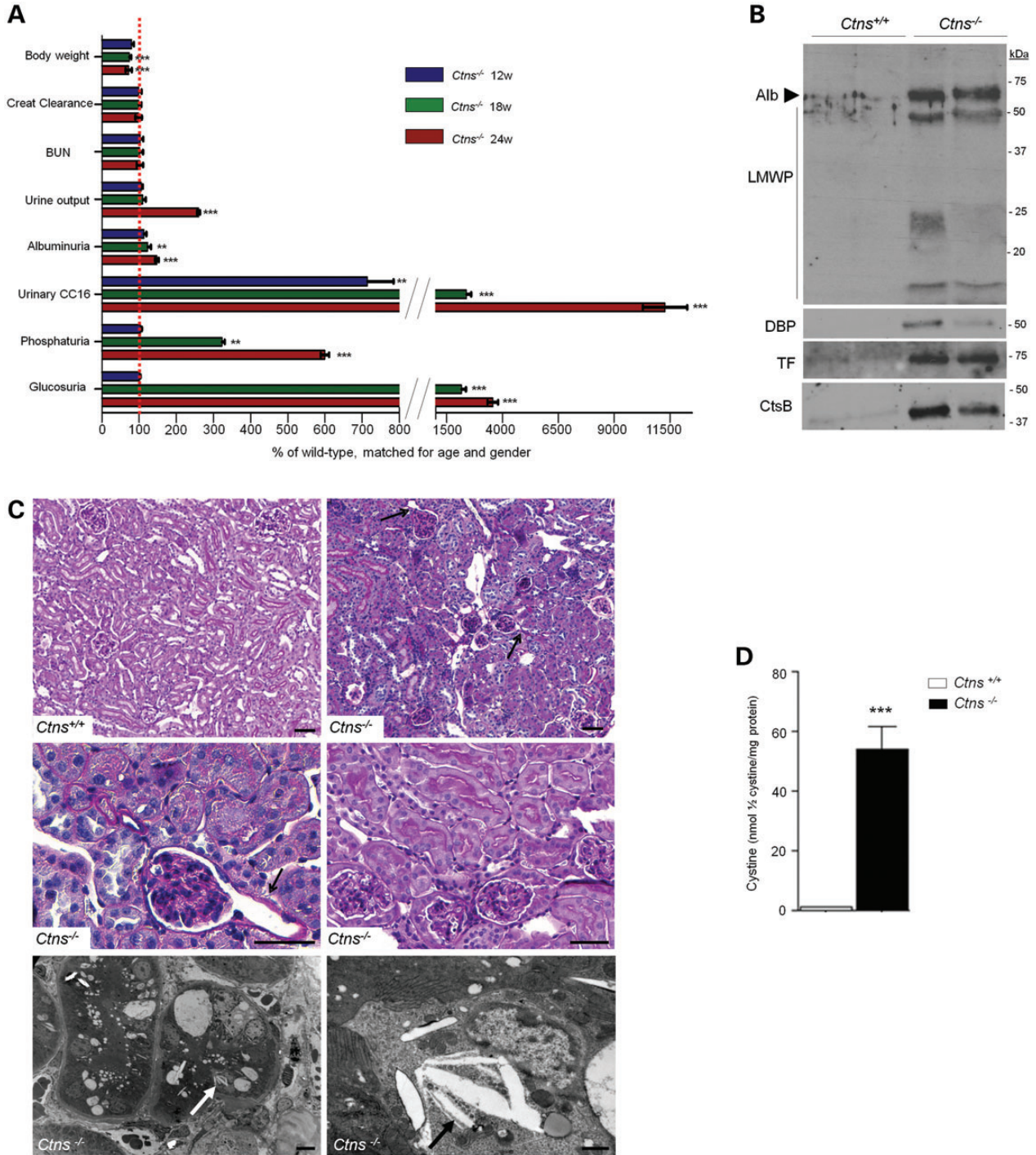
Figure 1. *Ctns* mouse model : progression of renal phenotype. (**A**) Growth retardation and evolution of PT dysfunction in *Ctns*$^{-/-}$ mice. From 12 weeks of age (blue bars), *Ctns*$^{-/-}$ mice present a trend for lower body weight than wild-type littermates, as well as increased urinary excretion of Clara cell protein (CC16), indicative of LMW proteinuria in the absence of renal failure (BUN and creatinine clearance). At age 18 weeks (green bars), *Ctns*$^{-/-}$ mice show significant growth retardation, with an increased urinary excretion of glucose, phosphate and albumin. At 24 weeks of age (red bars), *Ctns*$^{-/-}$ mice show a complete renal Fanconi syndrome, in the absence of signs of renal failure. All values are expressed as percentage of wild-type, matched for age and gender (*$P < 0.05$; **$P < 0.01$; ***$P < 0.001$). Ten pairs of *Ctns* mice were examined at each time point. (**B**) Urinary excretion of albumin (Alb, arrowhead), LMW proteins (LMWPs), vitamin D-binding protein (DBP), TF and procathepsin B (CtsB) in 24-week-old *Ctns* mice. Urine samples were loaded on 7.5% polyacrylamide gel electrophoresis, blotted to nitrocellulose and incubated with appropriate primary antibodies. Loading was normalized to urinary creatinine concentration. A major increase in urinary excretion of albumin and LMWP is detected in *Ctns*$^{-/-}$ mice. (**C**) Structure of the *Ctns* kidneys. Upper and middle panels: staining with periodic acid Shiff and hematoxylin on *Ctns* kidney sections obtained at 24 weeks of age. The *Ctns*$^{-/-}$ kidneys show the typical swan neck lesions (arrows) in <5% of nephrons. Otherwise, the renal parenchyma of *Ctns*$^{-/-}$ mice is normal. Lower panels: Electron microscopy of kidney cortex in 24-week-old *Ctns*$^{-/-}$ mouse reveals lysosomal accumulation of cystine crystals of various sizes in PT cells (arrows). Scale bar: 200 μm (top panels); 50 μm (middle panels); 5 μm (bottom left panel); 0.5 μm (bottom right panel). (**D**) Cystine levels assay in kidney cortex from 24-week-old *Ctns* mice. A major increase in the cystine levels is observed in *Ctns*$^{-/-}$ versus *Ctns*$^{+/+}$ kidneys (57.3 ± 2.8 versus 0.54 ± 0.04 nmol 1/2 cystine/mg protein, $n = 4$ pairs, ***$P < 0.001$).

Table 1. Body weight, plasma and urine parameters in the *Ctns* mice

	Body weight (g)	Urine volume (µl/24 h)	GFR (µl/min/g BW)	Urinary albumin (µM/mg creat/dl)	Urinary CC16 (µg/g creat)	Urinary Calcium (mg/g creat)	Urinary phosphate (mg/g creat)	Urinary Glucose (mg/g creat)	Urinary creat (mg/dl)	BUN (mg/dl)	Plasma Creat (mg/dl)
Ctns$^{+/+}$ (n = 10) Age : 12 weeks	21.7 ± 0.8	891 ± 105	51 ± 9	2746 ± 468	16 ± 6	13 ± 2	65 ± 8	1.5 ± 0.08	56 ± 4	36 ± 1	0.07 ± 0.004
Ctns$^{-/-}$ (n = 10) Age : 12 weeks	19.6 ± 0.4***	946 ± 117	50 ± 4	3087 ± 119	117 ± 37**	17 ± 6	77 ± 5	1.5 ± 0.12	53 ± 5	39 ± 2	0.08 ± 0.005
Ctns$^{+/+}$ (n = 10) Age : 18 weeks	24.5 ± 06	847 ± 125	50 ± 5	2547 ± 257	13 ± 4	12 ± 4	64 ± 6	1.3 ± 0.03	57 ± 3	38 ± 5	0.08 ± 0.001
Ctns$^{-/-}$ (n = 10) Age : 18 weeks	20.8 ± 0.2***	935 ± 109	51 ± 2	3157 ± 287**	309 ± 85***	15 ± 3	207 ± 11***	28 ± 5***	55 ± 6	32 ± 2	0.08 ± 0.002
Ctns$^{+/+}$ (n = 10) Age : 24 weeks	27.5 ± 0.9	840 ± 100	50 ± 7	2464 ± 250	9 ± 2	10 ± 1	68 ± 3	1.4 ± 0.05	61 ± 5	38 ± 2	0.08 ± 0.004
Ctns$^{-/-}$ (n = 10) Age : 24 weeks	22.6 ± 0.7**	1570 ± 105*	49 ± 3	4970 ± 543***	986 ± 202***	11 ± 3	398 ± 27***	49 ± 10***	51 ± 3	39 ± 3	0.08 ± 0.003

$*P < 0.05; **P < 0.01; ***P < 0.001$

D as a luminal marker (Fig. 4B). Importantly, confocal microscopy revealed that LAMP1-positive lysosomes were dispersed widely throughout the cytosol in control cells, whereas lysosomes aggregated predominantly in the perinuclear region of cystinosin-depleted cells (Fig. 4B).

Having shown that the loss of cystinosin function results in an accumulation of enlarged lysosomes in PT cells, we next examined whether the lysosomal enzymatic degradation capacity was affected. Dynamic and quantitative analysis of lysosomal enzymatic activity was performed by monitoring the temporal response of cathepsin B activity in live cells by fluorescence Recovery After Photo-bleaching (FRAP) experiments. To this end, living primary cultured PT cells from *Ctns* kidneys were loaded with the membrane-permeable substrate, Magic Red that, upon cathepsin B cleavage, releases fluorescent peptides inside lysosomes. In control *Ctns*$^{+/+}$ cells, photobleaching of Magic Red-positive lysosomes was followed by a rapid ($\tau_{1/2} = 47$ s) and substantial (60%) recovery of the initial fluorescence (Fig. 4F, upper panels). Conversely, in *Ctns*$^{-/-}$ cells, the fluorescence recovery was slower ($\tau_{1/2} = 60$ s) and smaller (20% recovery of the initial fluorescence) (Fig. 4F, lower panels). To confirm the specificity of the Magic Red tracer, we incubated *Ctns*$^{+/+}$ cells with leupeptin so to block specifically the cathepsin B activity (Fig. 4G). The treatment with leupeptin suppressed the release of fluorescent peptides, indicating that Magic Red hydrolysis was cathepsin B dependent.

Dedifferentiation, proliferation and defective transcriptional program in cystinosis

We next investigated potential mechanisms for the loss of PT receptors and transporters expression in the early phase of cystinosis. By analogy with other congenital or acquired disorders of the PT, we reasoned that such changes could reflect a dedifferentiated state of the epithelial cells due to a specific transcriptional program (12,13). The 24-week-old *Ctns*$^{-/-}$ kidneys showed a marked increase in the expression of the proliferation markers PCNA and cyclin D1 (Fig. 5A and B). Both molecules are classical targets of the Y-box transcription factor zonula occludens-1 (ZO-1)-associated nucleic acid-binding (ZONAB) protein (14), which showed a nuclear translocation (Fig. 5A) and co-enrichment with PCNA in nuclear extracts of *Ctns*$^{-/-}$ kidneys (Fig. 5C). The fact that ZONAB drives proliferation and directly represses megalin and cubilin in PT cells (13) could explain the functional changes observed in *Ctns*$^{-/-}$ mice.

The latter hypothesis was substantiated in PT cells obtained from *Ctns* mice (Fig. 6). The *Ctns*$^{-/-}$ cells showed increased proliferation (Fig. 6A), and a major nuclear translocation of ZONAB together with PCNA expression (Fig. 6B and C). Since the mRNA expression of ZONAB is unchanged in these cells, we tested whether the increased ZONAB activity could reflect a loss of tight junction integrity (14). The primary cultured PT cells obtained from *Ctns*$^{-/-}$ kidneys showed a loss of tight junction integrity as evidenced by a loss of signal for ZO1 (Fig. 6D and E) and a reduction in the transepithelial resistance (R_t: 26.2 ± 2.3 versus 58.4 ± 2.7 Ω/cm^2) and current (I_{sc}: 5.42 ± 0.76 versus 14.2 ± 0.63 µA/cm^2) compared with control cells (Fig. 6F).
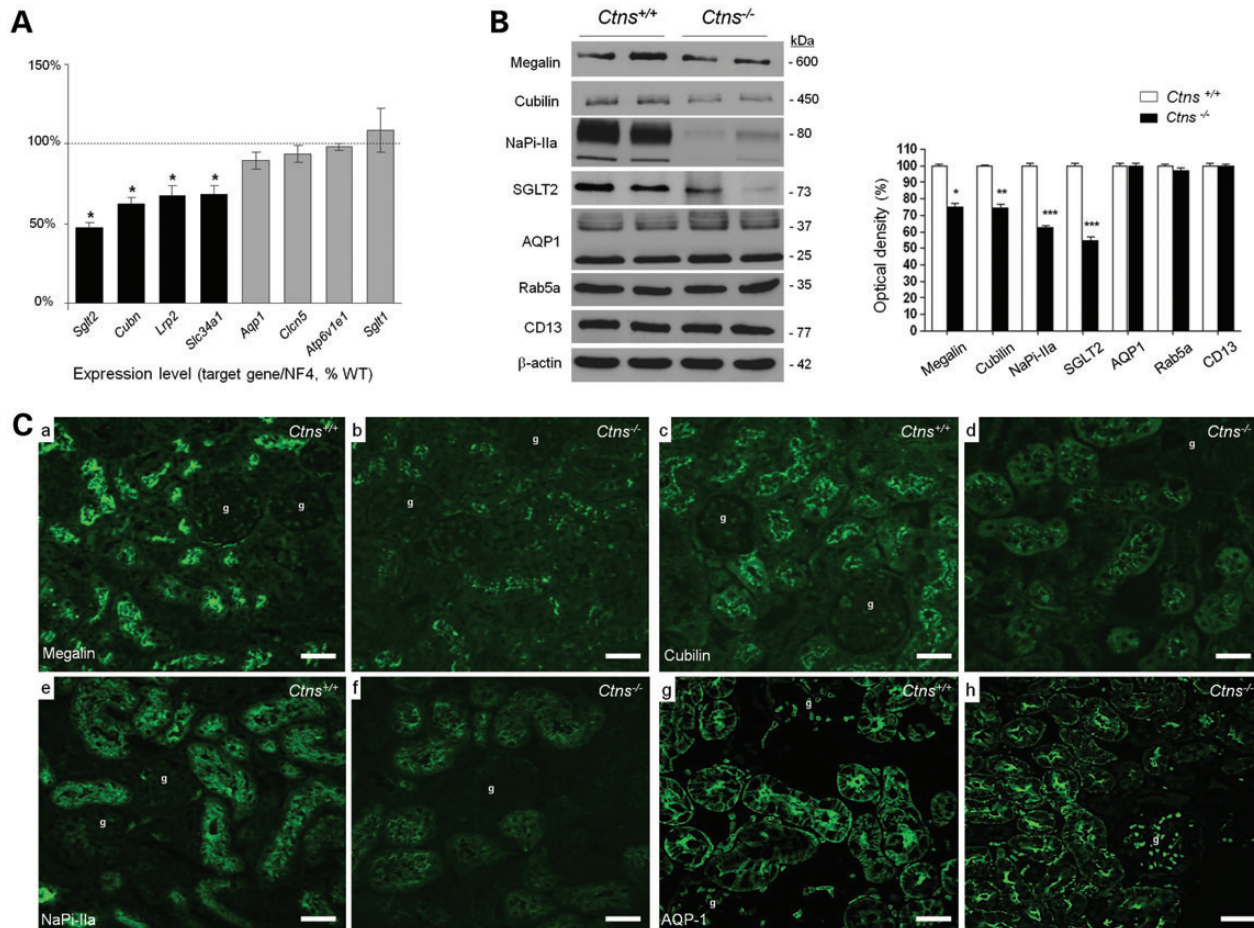
Figure 2. *Ctns* kidneys: expression of endocytic markers. (**A**) Quantitative RT–PCR to measure the mRNA expression of PT genes (*Aqp1, Lrp2, Cubn, Clcn5, Sglt2, Sglt1, Slc34a1 and Atp6v1e1*) mRNA in 24-week-old, whole *Ctns* kidneys ($n = 7$ pairs). A decreased expression of *Lrp2* (megalin), *Cubn* (cubilin), *Sglt2* (SGLT2) and *Slc34a1* (NaPi-IIa) mRNA is observed in *Ctns*$^{-/-}$ kidneys versus *Ctns*$^{+/+}$ controls (taken as 100%, dotted line). The mRNA expression of target genes was normalized to the normalization factor calculated from four different housekeeping genes. Values are expressed as mean $\pm$ SEM, *$P < 0.05$. (**B**) Representative immunoblotting and densitometry analysis for PT markers megalin, cubilin, NaPi-IIa, AQP1, Rab5a and CD13 in 24-week-*Ctns* kidneys ($n = 4$ pairs). Equal amounts of protein extracts (20 µg) were run on SDS–PAGE, transferred to nitrocellulose and probed with appropriate antibodies. Membranes were stripped and reincubated for β-actin. The expression of megalin, cubilin and NaPi-IIa is reduced in *Ctns*$^{-/-}$ extracts, whereas the expression of AQP1, Rab5a and CD13 is unchanged versus *Ctns*$^{+/+}$. Densitometry values are expressed as mean $\pm$ SEM, *$P < 0.01$; **$P < 0.001$; ***$P < 0.0001$. (**C**) Immunofluorescence staining for megalin (a, b), cubilin (c, d), NaPi-IIa (e, f) and AQP1 (g, h) in *Ctns*$^{+/+}$ (a, c, e, g) and *Ctns*$^{-/-}$ (b, d, f, h) kidneys from 24-week-old mice. The signal for megalin, cubilin and NaPi-IIa is strongly reduced in the PT of *Ctns*$^{-/-}$ kidneys, whereas staining for AQP1 is unchanged. Scale bar: 50 µm.

DISCUSSION

In this study, we show that invalidation of cystinosin in mouse induces a progressive dysfunction of the PT with LMW proteinuria, glucosuria and phosphaturia, *before* structural damage and *in the absence* of renal failure. These changes are related to aberrations in the endolysosomal compartment, with decreased expression of megalin and cubilin receptors and of specific transporters, in parallel with dedifferentiation and increased proliferation of PT cells. Studies on primary cultures of PT cells confirmed both the defective endocytosis and the impaired lysosomal function, with a loss of integrity of tight junctions and an abnormal transcription program involving ZONAB. These data reveal that, like other types of lysosomal storage disorders, cystinosis is associated with aberrations affecting the endolysosomal compartment (15,16).

In addition to glucose, amino acids, phosphate and other ions, a significant amount of filtered albumin and LMW plasma proteins is continuously reabsorbed by the epithelial cells lining the PT. The uptake of LMW proteins by these cells essentially involves receptor-mediated endocytosis, while fluid-phase capture can be considered as quantitatively negligible. The process essentially requires two multiligand receptors, megalin and cubilin, and the cooperating protein amnionless that are expressed at the brush border of the cells (17). Ligand binding and interactions between both receptors induce their internalization into coated vesicles and their subsequent delivery to endosomes and lysosomes for ligand processing and receptor degradation or recycling. Over the past 15 years, the molecular analysis of rare inherited diseases identified defective receptor-mediated endocytosis as a major mechanism of renal Fanconi syndrome (17–19). Selective proteinuria and manifestations of
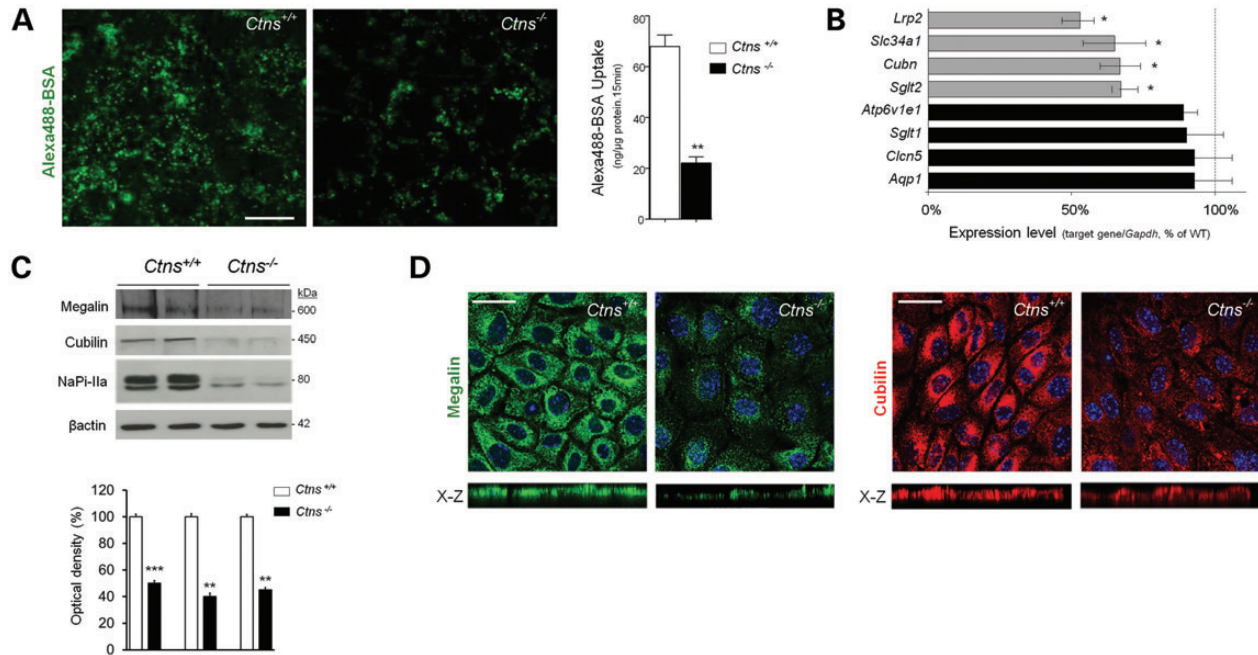
Figure 3. Defective endocytosis in PT cells from *Ctns$^{-/-}$* kidneys. (**A**) Confluent monolayers of primary cultures of PT cells obtained from 20-week-old *Ctns* kidneys were incubated with 0.5 mg/ml Alexa488-conjugated BSA for 1 h at 4°C, followed by 15 min incubation with growth medium at 37°C. A decreased uptake of Alexa488-BSA is observed in *Ctns$^{-/-}$* cells compared with control cells (left panel; scale bar: 10 μm). The uptake of Alexa488-BSA was quantified in a single-beam fluorimeter (right panel), confirming the major decrease in PT cells from *Ctns$^{-/-}$* versus *Ctns$^{+/+}$* (23.5 ± 5.0 versus 74.7 ± 7.2 ng/μg protein.15 min, respectively, **$P < 0.01$). (**B**) Quantitative RT-PCR to assess the expression of PT markers in primary cultures of PT cells obtained from 20-week-old *Ctns$^{-/-}$* kidneys (compared with levels in *Ctns$^{+/+}$* cells taken as 100%). The mRNA expression of target genes was normalized to *Gapdh*. The *Ctns$^{-/-}$* cells show a decreased expression of *Lrp2*, *Slc34a1*, *Cubn*, *Sglt2* mRNA versus *Ctns$^{+/+}$* cells. Values are expressed as mean ± SEM, *$P < 0.05$ ($n = 6$ pairs). (**C**) Immunoblotting and densitometry analysis for megalin, cubilin and NaPi-IIa in primary cultures of PT cells from *Ctns$^{+/+}$* versus *Ctns$^{-/-}$* kidneys. Equal amounts of proteins (15 μg) from cell cultures (six wells/sample) were loaded on each lane. The expression of megalin, cubilin and NaPi-IIa is decreased in *Ctns$^{-/-}$* cells compared with wild-type. Values are expressed as mean ± SEM, $n = 5$ pairs of samples, **$P < 0.01$; ***$P < 0.001$. (**D**) Monolayers of PT cells from *Ctns$^{+/+}$* and *Ctns$^{-/-}$* kidneys were labeled with antibodies against megalin (green, left panel) and against cubilin (red, right panel). Confocal microscopy images (upper panels) and X–Z side view of a z-stack (bottom panels) reveal a decreased expression of megalin and cubilin at the apical plasma membrane in *Ctns$^{-/-}$* PT cells compared with wild-type cells. Nuclei counterstained with DAPI (blue). Scale bar, 10 μm.

PT dysfunction are detected in patients and corresponding mouse models with inactivating mutations in *LRP2* coding for megalin (Donnai–Barrow syndrome) (20), in *CUBN* coding for cubilin or *AMN* coding for amnionless (Imerslund–Gräsbeck syndrome) (21), and the *CLCN5* gene coding for the endosomal exchanger ClC-5 (Dent's disease) (19). Despite evidence of PT dysfunction and renal Fanconi syndrome, the potential involvement of megalin and cubilin in the pathogenesis of nephropathic cystinosis has been questioned (5), relying on expression studies in renal biopsies (8) and clonal cells derived from the urine (6).

Based on several lines of evidence, our studies demonstrate that receptor-mediated endocytosis is involved in the PT dysfunction associated with cystinosis. Detailed metabolic studies performed every 4 weeks allowed us to establish the time course of tubular dysfunction in *Ctns$^{-/-}$* mice. These mice show progressive manifestations of renal Fanconi syndrome (LMW proteinuria including albumin and specific ligands of megalin and cubilin, phosphate and glucose) from 12 weeks to 20 weeks, in the absence of renal failure or major histology lesions. The fact that <5% of nephrons show swan-neck lesions in the S1 segment at this stage indicate that the urinary loss of solutes is not caused by a loss of tubular functional mass, but rather by a specific mechanism in apparently intact cells. The nature of this mechanism was

further investigated by using well-established primary cultures of PT cells obtained from *Ctns$^{-/-}$* kidneys. When grown on filters, these cells polarize and keep their differentiation as shown by morphological features and specific transport processes (11). The primary cultures are obtained from defined PT segments, at very precise stages of disease and with matched control cells from littermates. The primary cells are particularly well-suited to investigate receptor-mediated endocytosis and lysosomal processing, as recently shown in mice KO for megalin (12) and ClC-5 (22), two models that are directly relevant for nephropathic cystinosis.

Analyses of PT cells obtained from *Ctns$^{-/-}$* kidneys reveal that their functional defect includes both defective endocytosis and impaired lysosomal processing. These changes are caused by a selective decrease in the expression of megalin and cubilin as well as cystine accumulation leading to enlarged, perinuclear lysosomes. The lysosomal defect is evidenced by the strong decrease in cathepsin B activity revealed by FRAP analysis. Importantly, the PT phenotype of the *Ctns$^{-/-}$* mice includes the urinary loss of cathepsin B, as was already observed for the *Clcn5$^{-/-}$* mice that mimic Dent's disease (23). Of note, these defects do not involve endosome catalysts (Rab5a) and components of the brush border membrane (CD13), nor the lysosome-associated
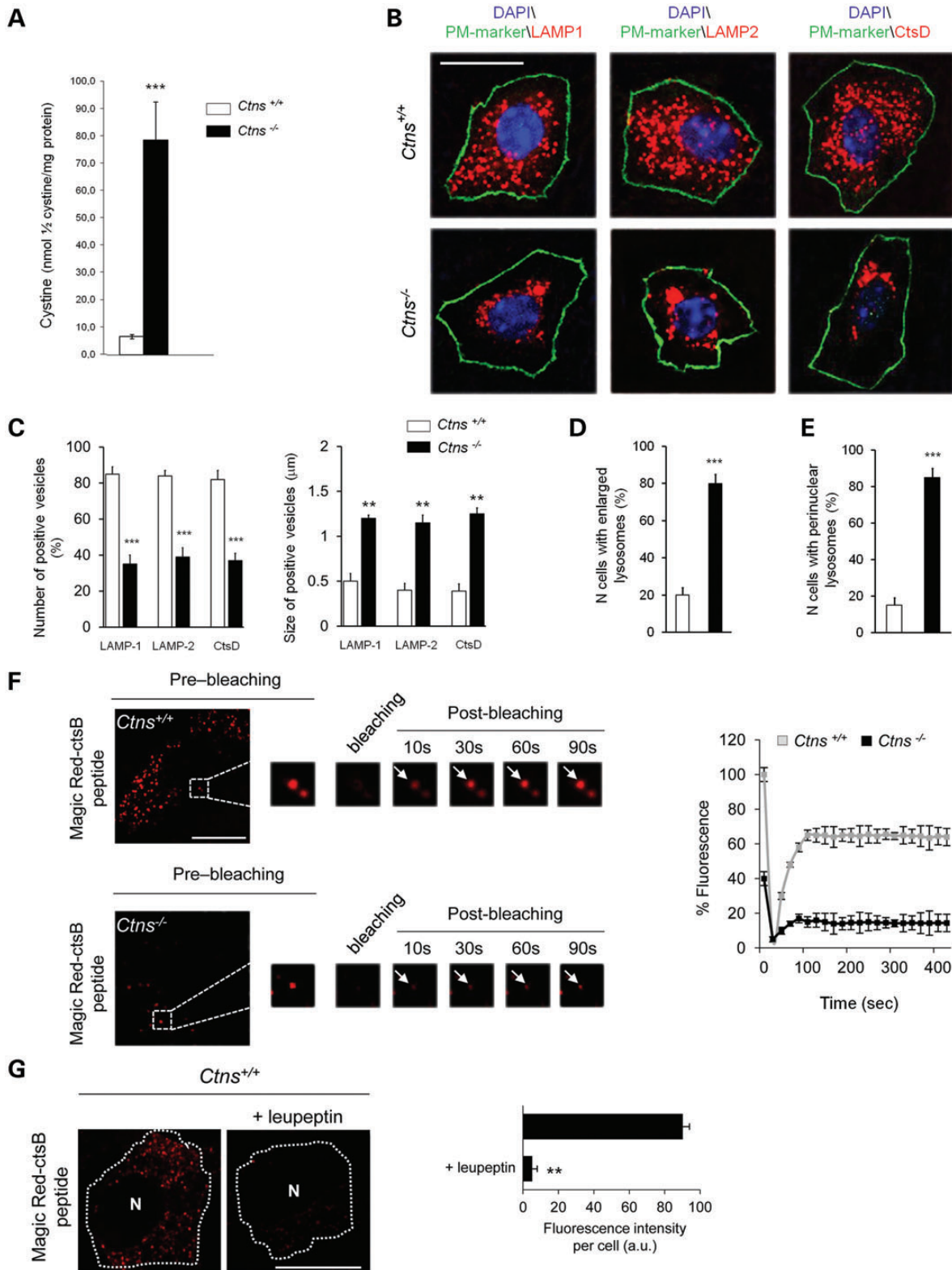
Figure 4. Lysosomal dynamic and degradative capacity are altered in PT cells from $Ctns^{-/-}$ kidneys. (**A**) Intracellular cystine assay in primary culture of PT cells isolated from 20-week-old *Ctns* kidneys ($N = 6$ samples). A major increase in intracellular cystine levels is observed in $Ctns^{-/-}$ cells versus controls (78.7 ± 13.9 versus 5.1 ± 1.4 nmol 1/2 cystine/mg protein, respectively, $n = 4$ pairs of samples, ***$P < 0.001$). (**B**) Primary cultured PT cells from *Ctns* kidneys were labeled with antibodies against plasma membrane and lysosome markers in order to evaluate the steady-state distribution of LAMP1, LAMP2 and cathepsin D (CtsD). Representative images of $Ctns^{-/-}$ PT cells show a significant decrease in the number and an increase in the size of LAMP1-, LAMP2- and CtsD-positive vesicles, in comparison with $Ctns^{+/+}$ cells. Nuclei counterstained with DAPI (blue). Scale bar, 10 µm. C-E. The cells from (B) were assessed in a blind fashion for (**C**) change in number and size of LAMP1, LAMP2 and CtsD-positive vesicles, for (**D**) presence of enlarged lysosomes; and for (**E**) change in vesicle positioning. Values are expressed as

proteins LAMP1 and LAMP2 (data not shown). The endocytic defect in nephropathic cystinosis is thus very similar to that encountered in Dent's disease (24), indicating that the functional loss of an endosomal chloride–proton exchanger (ClC-5) or of a lysosomal transporter (cystinosin) may have the same functional consequences on the endolysosomal compartment in PT cells.

In addition to receptor-mediated endocytosis, a second distinct pathway operating at the apical border of PT cells appears to be defective in this cystinosis model. Indeed, $Ctns^{-/-}$ mice show phosphaturia and a decreased expression of NaPi-IIa cotransporter in PT cells. It must be noted that LMW proteinuria occurs at least 4 weeks before phosphaturia in the $Ctns^{-/-}$ mice. Since phosphate reabsorption via NaPi-IIa is under the control of the parathyroid hormone (PTH) via its receptors (PTHR) located on the apical and basolateral poles of the cells, one can hypothesize that a trafficking defect similar to that observed in $Clcn5^{-/-}$ kidneys *ex vivo* (23) and *in vivo* (25) may be involved.

Our previous studies have shown that transcription factors play an important role in the phenotypic changes observed in PT cells in various types of renal Fanconi syndromes (13,14,26). In particular, the Y-box transcription factor (ZONAB) protein promotes cell proliferation (by inducing the expression of the proliferating factors PCNA and cyclin D1) but directly represses megalin/cubilin expression in PT cells (14). Our data show that the mRNA expression of megalin/cubulin is decreased in $Ctns^{-/-}$ kidneys and primary cultured cells, whereas the nuclear expression of ZONAB is increased. Furthermore, PCNA and cyclin D1, which are direct targets of ZONAB, are also increased. The $Ctns^{-/-}$ cells are consistently hyperproliferative, whereas additional markers of dedifferentiation are strongly increased. These data suggest that the loss of cystinosin is associated with a switch between differentiation and proliferation, which may involve a specific transcriptional cascade in PT cells. Dedifferentiation would be reflected by decreased expression of megalin/cubilin, causing defective endocytosis and LMW proteinuria. Alternatively, the switch towards proliferation could involve the loss of lysosomal function. It is known that retention inside the endolysosomal compartment with subsequent prolonged activation of the EGF-receptor may cause dedifferentiation in renal PT cells (27). Future studies using a multi-level approach based on transcriptomics, proteomics and metabolomics will be necessary to understand how the dysregulated transcriptional program induced by the functional loss of cystinosin may have an impact on key proteins involved in the functions of PT cells.

In summary, our data reveal that the loss of cystinosin function in PT cells triggers an abnormal transcription program with profound defects in the endolysosomal pathway leading to the urinary loss of specific ligands, before structural damage or renal failure. Insights into the early manifestations of nephropathic cystinosis may offer new targets for intervention, before irreversible renal damage.

MATERIALS AND METHODS

Transgenic mice

All experiments were conducted on age- and gender-matched $Ctns^{+/+}$ and $Ctns^{-/-}$ littermates (C57BL/6 background) (10). The mice had free access to appropriate standard diet (Carfil Quality, Oud-Turnhout, Belgium). All procedures were performed in accordance with National Institutes of Health guidelines for the care and use of laboratory animals and with the approval of the Committee for Animal Rights of the UCL Medical School (Brussels, Belgium) and the University of Zurich (Zurich, Switzerland).

Renal function parameters

After genotyping at 6 weeks, mice were trained and kept once weekly in metabolic cages (overnight) with ad libitum access to food and drinking water. The urine was collected over ice and diuresis was measured. Blood (intracardiac puncture) and kidneys were obtained after anesthesia with ketamine/xylazine or isoflurane (23,24). The urine and blood parameters were measured using a Synchron CX5 analyzer (Beckman Coulter, Fullerton, CA, USA), whereas Clara cell protein (CC16) concentration was measured in duplicate by latex immunoassay (courtesy of X. Dumont, UCL Medical School, Brussels, Belgium). Urinary LMW proteins, including vitamin D-binding protein and transferrin (TF) were measured by western blotting as described previously (23,24,28,29).

Histological studies

Kidneys from the *Ctns* mice were rapidly dissected, rinsed in ice-cold PBS, fixed in 4% paraformaldehyde in 0.1 M phosphate buffer for 6 h, and embedded in paraffin. Sections were deparaffinized with xylene and rehydrated with descending ethanol into PBS, then stained with hematoxylin and eosin analyzed and photographed with an Axioplan2 microscope (Carl Zeiss, Zaventem, Belgium) and an AxioCam camera (Carl Zeiss). Sections were read by a renal pathologist blinded to the animal group. For ultrastructural examination, kidney samples were fixed with 4% glutaraldehyde in PBS at 4°C for 2 h. After washing with 0.1 M PBS, samples were post-fixed with 1% osmium tetroxide, dehydrated and embedded in araldite. Ultrathin sections were examined with a JEOL 1010 transmission electron microscope (JEOL, Tokyo, Japan) after uranyl acetate and lead citrate staining.

---

mean $\pm$ SEM ($n = 50$ cells; three independent experiments; ***$P < 0.001$ (number) and **$P < 0.01$ (size); ***$P < 0.001$ (enlarged lysosomes) and **$P < 0.01$ (positioning). (**F**) FRAP assay of cathepsin B activity. Time-lapse of photo-bleaching and fluorescence recovery of Magic Red-positive lysosomes in primary PT cells from $Ctns^{+/+}$ (upper panels) and $Ctns^{-/-}$ (lower panels) cells. Representative images, with time intervals indicated in seconds. Right panel: FRAP analysis of Magic Red-positive lysosomes from $Ctns^{-/-}$ and $Ctns^{+/+}$ PT cells. The FRAP data are displayed as percentage of recovery with respect to the fluorescence before bleach (100%) and are representative of 10 recordings from different cells. The fluorescence recovery is significantly attenuated in $Ctns^{-/-}$ cells as compared with control $Ctns^{+/+}$ cells ($\tau_{1/2}$, time for exchanging half of the mobile Magic Red fraction between bleached and unbleached areas: 68 ± 3.5 versus 47 ± 2.9 s, respectively, $P < 0.05$). (**G**) Validation of the Magic Red-cathepsin B assay. Representative image of treatment with 100 μM leupeptin [in dimethyl sulfoxide (DMSO)] on $Ctns^{+/+}$ PT cells exposed to Magic Red-cathepsin B: a decreased degradation capacity of lysosomes is observed in $Ctns^{+/+}$ cells exposed to leupeptin compared with DMSO alone. Scale bar, 10 μm. Right panel: quantification of cell-associated Magic Red vesicles, evaluated as mean fluorescence intensities per cell and expressed in arbitrary units (a.u.; $n = 50$ cells; three independent experiments, **$P < 0.001$).
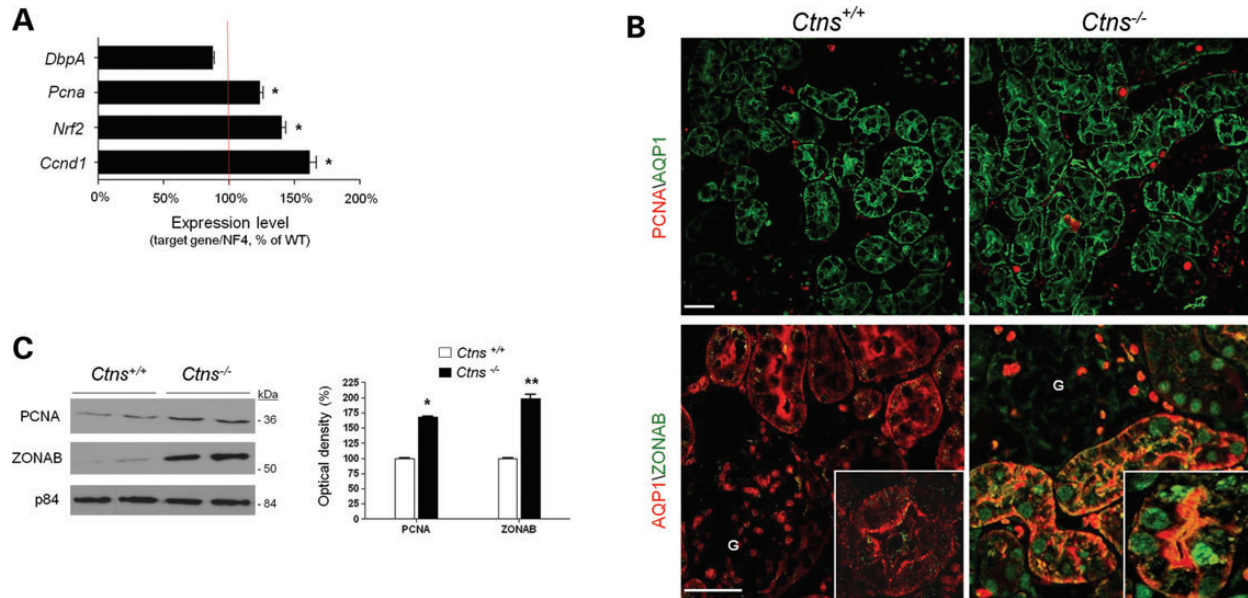
Figure 5. *Ctns*^{−/−} kidneys: dedifferentiation and proliferation. (**A**) Quantitative RT-PCR analysis of the expression of the proliferation markers *Pcna* (PCNA) and *Ccnd1* (Cyclin D1) and the transcription factors *Nrf2* (NRF2) and *DbpA* (ZONAB) mRNA in whole kidneys, obtained from 24-week-old *Ctns* mice ($n = 7$ pairs). The *Ctns*^{−/−} kidneys show an increased expression of PCNA, CyclinD1, and NRF2 in comparison with *Ctns*^{+/+} samples (*$P < 0.05$). (**B**) Upper panels: Double immuno-fluorescence staining for PCNA and AQP1 in 24-week-old *Ctns* kidneys. An increased nuclear expression of PCNA is observed in the AQP1-positive PT cells of *Ctns*^{−/−} kidneys, demonstrating an increased cellular proliferation. Lower panels: Immunofluorescence for ZONAB and AQP1 in 24-week-old *Ctns* kidneys. In comparison with wild-type tissue, *Ctns*^{−/−} kidneys show a nuclear concentration of ZONAB in AQP1-positive PT cells. G, glomeruli (AQP1 in erythrocytes). Scale bar 50 μm. (**C**) Representative immunoblotting of nuclear extracts from 24-week-old *Ctns* kidneys showing increased expression of ZONAB and PCNA in nuclei from *Ctns*^{−/−} kidneys. Loading control was performed after membrane stripping and incubation with monoclonal antibody against nuclear matrix protein p84. Values are expressed as mean ± SEM on four pairs of samples. (*$P < 0.05$; **$P < 0.01$).

Antibodies

The following antibodies were used in this study: mouse anti-rat PCNA (Dako, Glostrup, Denmark), rabbit anti-human DBP (Dako), rabbit anti-human LMW proteins (Dako), rabbit anti-human CC16 (BioVendor, Heidelberg, Germany), rabbit anti-human TF (Dako); goat anti-mouse cathe-psin B/D (R&D, Minneapolis, USA); mouse anti- β-actin (Sigma, St. Louis, USA); rabbit anti-human ZO1 (Invitrogen, Life Technologies, Zug, Switzerland); rabbit anti-mouse and anti-human ZONAB (Invitrogen; Bethyl Lab, Montgomery, USA), rabbit anti-human AQP1 (Millipore, Billerica, USA), rabbit anti-human CD13 (Abcam, Cambridge, UK), mouse anti-human nuclear matrix protein p84 (Abcam), rabbit anti-NaPi-IIa (gift from C. A. Wagner, University of Zurich, Zurich), rabbit anti-mouse Rab5a (Sigma), rabbit anti-rat LAMP1 (Abcam), rabbit anti-rat LAMP2 (Abcam). Sheep anti-megalin and rabbit anti-cubilin were kindly provided by Dr. P. Verroust, INSERM, Paris, France.

Isolation and primary cultures of PT cells

Primary cultures of mouse PT cells were prepared from gender-matched *Ctns*^{+/+} and *Ctns*^{−/−} mice aged of 20 weeks as described previously (11). For the isolation of PT cells, PT segments were seeded onto collagen-coated PTFE filter membranes (0.33 cm², pore size 0.4 μm, Transwell-COL[TM], Costar[TM], Corning Inc., USA) in culture medium (DMEM:F12 with 15 mM HEPES, 0.55 mM Na-pyruvate, 0.1 ml/l non-essential amino acids and the SingleQuots® kit (Lonza, Verviers, Belgium) containing hydrocortisone, hEGF, FBS, epinephrine, insulin, triiodothyronine, TF, gentamicin/amphotericin, pH 7.40, 325 mOsm/kg) and incubated in a humidified chamber at 37°C−5% CO_2. The medium was replaced every 48 h. Confluent monolayers of PT cells expanded from the tubular fragments after 6−7 days. All experiments were performed on non-passaged, confluent monolayers grown on collagen-coated filters.

Quantitative real-time PCR

Total RNA was extracted from kidneys using AurumTM Total RNA Fatty and Fibrous Tissue Kit (Bio-Rad, Hercules, CA), following the manufacturer's protocol. DNAse I treatment was performed to eliminate genomic DNA contamination. Total RNA was extracted from primary cell cultures with RNAqueousR kit (Applied Biosystems, Life Technologies), following the manufacturer's protocol. One microgram of RNA was used to perform the reverse transcriptase reaction with iScriptTM cDNA Synthesis Kit (Bio-Rad). The primers were designed using Beacon Designer 2.0 (Premier Biosoft International, Palo Alto, USA) (Table 2). Changes in target genes mRNA levels were determined by quantitative reverse transcriptase-polymerase chain reaction (RT-PCR) with an iCycler IQ System (Bio-Rad) using SYBR Green I detection of single PCR product accumulation. The qRT-PCR analyses were performed in duplicate with 100 nM of both sense and anti-sense primers in a final volume of 20 μl using iQTM SYBR Green Supermix
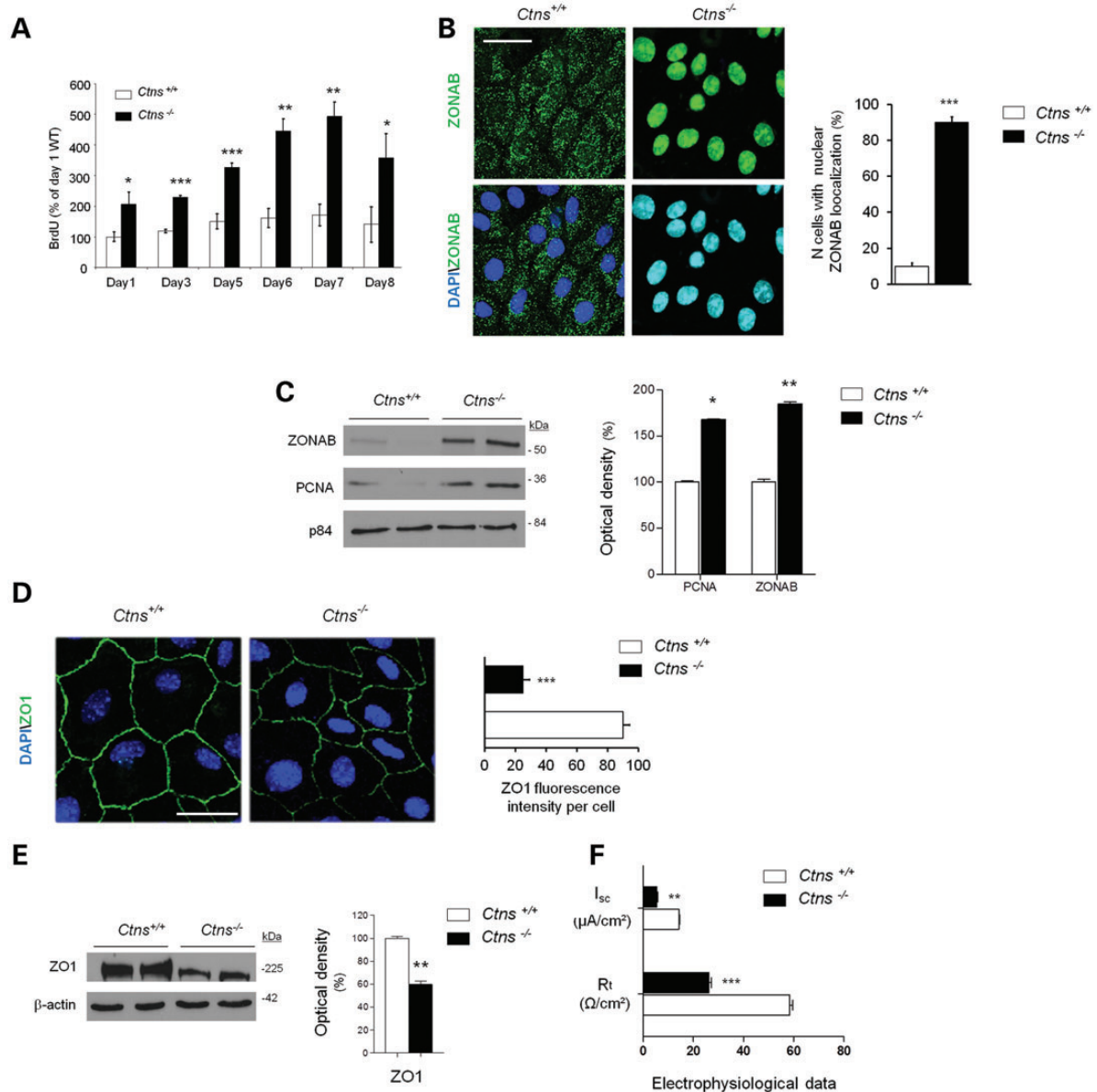
Figure 6. Proliferation and dedifferentiation in PT cells from $Ctns^{-/-}$ kidneys. (**A**) Time-course of BrdU incorporation in primary cultures of PT cells obtained from $Ctns$ kidneys. Increased cell proliferation was detected in $Ctns^{-/-}$ versus wild-type cells at each time point. Values are expressed as mean $\pm$ SEM, $n = 4$ pairs of samples. *$P < 0.05$, **$P < 0.01$, ***$P < 0.001$. (**B**) Immunofluorescence for ZONAB in primary cultures of PT cells from $Ctns$ kidneys. Left panels: Representative images showing nuclear translocation of ZONAB in $Ctns^{-/-}$ cells compared to diffuse cytoplasmic staining in $Ctns^{+/+}$ cells. Nuclei counterstained with DAPI (blue). Scale bar, 10 µm. Right panels: Quantification of the number of cells with nuclear ZONAB. ($n = 50$ cells; three independent experiments, ***$P < 0.001$). (**C**) Immunoblotting and quantification for ZONAB and PCNA in primary cultured PT cells obtained from $Ctns^{+/+}$ and $Ctns^{-/-}$ kidneys. Equal amounts of proteins (15 µg) from nuclear extracts (six wells/sample) were loaded in each lane. The expression of ZONAB and PCNA is increased in $Ctns^{-/-}$ cells, compared with $Ctns^{+/+}$ cells. Values are expressed as mean $\pm$ SEM, *$P < 0.05$; **$P < 0.01$. (**D**) Immunofluorescence for the tight junction protein ZO1 in primary cultures of PT cells obtained from $Ctns$ kidneys. Left panels: The steady-state distribution of ZO1 is altered in $Ctns^{-/-}$ versus wild-type $Ctns^{+/+}$ cells. Nuclei counterstained with DAPI (blue). Scale bar, 10 µm. Right panel: Quantification of cell-associated ZO1, evaluated as mean fluorescence intensity per cell and expressed in arbitrary units (au; $n = 50$ cells; three independent experiments, ***$P < 0.001$). (**E**) Immunoblotting and quantification of ZO1 in PT cells from $Ctns$ kidneys. Equal amounts of proteins (15 µg) from 7-day-old primary cultured cells (six wells/sample) were loaded on SDS–PAGE, transferred to nitrocellulose and probed with anti-ZO1 antibodies. Loading was normalized for β-actin. The expression of ZO1 is decreased in $Ctns^{-/-}$ cells, compared with wild-type cells. Values are expressed as mean $\pm$ SEM, **$P < 0.01$. (**F**) Short-circuit current (I_{sc}) and transepithelial resistance (R_t) measured simultaneously on 7-day-old monolayers of primary cultured PT cells ($n = 5$) isolated from 20-week $Ctns^{+/+}$ (white bar) and $Ctns^{-/-}$ (black bar) mice. A strong reduction in I_{sc} (5.4 $\pm$ 0.76 versus 14.2 $\pm$ 0.63 µA/cm²) and R_t (26.2 $\pm$ 2.3 versus 58.4 $\pm$ 2.7 Ω/cm²) is observed in $Ctns^{-/-}$ versus $Ctns^{+/+}$ cells. **$P < 0.01$; ***$P < 0.001$.

(Bio-Rad). PCR conditions were 94°C for 3 min followed by 40 cycles of 30 s at 95°C, 30 s at 61°C and 1 min at 72°C. The relative changes in target gene/GAPDH mRNA ratio were determined by the relation $2^{-\Delta\Delta Ct}$ (30).

Western blotting

Protocol used for immunoblotting has been described previously (28,29). Proteins were extracted from isolated kidneys or

Table 2. Primers used for quantitative RT-PCR analyses

Gene product	Forward primer (5′–3′)	Reverse primer (5′–3′)	PCR product (bp)	Efficiency
Aqp1	GCTGTCATGTACATCATCGCCCAG	AGGTCATTGCGGCCAAGTGAAT	107	0.99 ± 0.02
Hspa1a	ACCACCTACTCGGACAACCA	CGAAGGTCACCTCGATCTGT	151	1.02 ± 0.03
Car3	TGACCCTGGCTCTGCTAAGA	AGCCCCAGTGAAGATGGAAT	178	$1.01\ 0.02$
Atp6v1e1	GGCGCTCAGCGATGCAGATGT	CAAGGCGACCTTTCTCAATG	134	1.05 ± 0.01
Sglt1	GTATGGTATGGTGGCCGATT	AATATCCAGCCCAGCACAAC	157	0.99 ± 0.02
DbpA	AGGACGCGGAGAAGAAAGTT	ACTTGCGTGGGTTGTTTTTC	153	0.96 ± 0.04
Pcna	TTGGAATCCCAGAACAGGAG	ATTGCCAAGCTCTCCACTTG	155	1.00 ± 0.03
Nrf2	CAGCCAGCTGACCTCCTTAG	TCAATAGTCCCGTCCAGGAG	159	1.02 ± 0.03
Ccnd1	AGCAGAAGTGCGAAGAGGAG	CAAGGGAATGGTCTCCTTCA	151	1.01 ± 0.03
Car2	CTTGAAGCACTGCATTCCAT	CACGATCCAGGTCACACATT	154	1.02 ± 0.03
Hmox1	AAGAGGCTAAGACCGCCTTC	TCTCTGCAGGGGCAGTATCT	153	1.01 ± 0.02
Sglt2	TTGGGCATCACCATGATTTA	GCTCCCAGGTATTTGTCGAA	164	1.02 ± 0.02
Cubn	TCATTGGCCTCAGACATTCC	CCCAGACCTTCACAAAGCTG	149	1.04 ± 0.02
Lrp2	CAGTGGATTGGGTAGCAGGA	GCTTGGGGTCAACAACGATA	150	1.01 ± 0.03
Slc34a1	CATCACAGAGCCCTTCACAA	TGGCCTCTACCCTGGACATA	161	0.98 ± 0.03
Clcn5	TGGAGGAGCCAATCCCTGGTGT	AGAAAGCATCGCTCACACTG	156	0.99 ± 0.02
Ppiase	CGTCTCCTTCGAGCTGTTTG	CCACCCTGGCACATGAATC	139	1.02 ± 0.02
Hprt1	ACATTGTGGCCCTCTGTGTG	TTATGTCCCCCGTTGACTGA	162	0.99 ± 0.01
Actb	TGCCCATCTATGAGGGCTAC	CCCGTTCAGTCAGGATCTTC	102	1.02 ± 0.02
Gapdh	TGCACCACCAACTGCTTAGC	GGATGCAGGGATGGGGGAGA	176	1.04 ± 0.03
Arbp	CTTCATTGTGGGAGCAGACA	TTCTCCAGAGCTGGGTTGTT	150	0.99 ± 0.01

primary cultured cells, lysed in lysis buffer containing protease inhibitors (Complete Mini^R, Roche Diagnostics, Belgium), followed by sonication and centrifugation at 16 000 *g* for 1 min at 4°C. Tissue, cell and urine samples were thawed on ice, normalized for protein (20 μg/lane) or urinary creatinine levels, diluted in Laemmli buffer and separated by sodium dodecyl sulphate–polyacrylamide gel electrophoresis (SDS–PAGE) in reducing conditions. After blotting onto nitrocellulose and blocking, membranes were incubated overnight at 4°C with primary antibody, washed, incubated with peroxidase-labeled secondary antibody, and visualized with enhanced chemiluminescence (ECL Pierce). For reprobing, the membranes were rinsed, incubated for 30 min at 55°C in a stripping buffer (62.5 mmol/l Tris-HCl, 2% SDS, 100 mM - mercaptoethanol, pH 7.4), before incubation with primary antibodies. Quantitative analysis was performed by scanning the blots and measuring the relative density of each band normalized to β-actin using NIH-Image V1–57 software.

Immunofluorescence and confocal imaging

Mouse kidneys were snap-frozen in cryogenic Tissue-Tek OCT compound (Electron Microscopy Sciences, Hatfield, USA). The embedded tissue was sectioned at 6 μm with a Leica cryostat (Leica, Heerbrugg, Switzerland). The sections were fixed with 4% paraformaldehyde, blocked with PBS containing 5% BSA, and incubated for 1 h with primary antibodies. After three PBS rinses, fluorophore-conjugated Alexa secondary antibodies (Invitrogen) were applied for 30 min. Sections were subsequently mounted in Prolong Gold Anti-fade reagent (Invitrogen) and then analysed under a Zeiss LSM510Meta Confocal microscope (Carl Zeiss).

The cells were fixed for 10 min with 4% paraformaldehyde (Sigma) in PBS, quenched with 50 mM NH4Cl and permeabilized for 30 min in blocking buffer (0.1% (w/v) Triton X-100, 0.5% (w/v) BSA in PBS/Ca/Mg). The cells were incubated for

2 h with the primary antibody, washed three times in PBS, incubated for 1 h with the secondary (Alexa labelled) antibody, washed three times in PBS and were finally taken on Vectashield-mounted coverslips. The samples were examined under a Zeiss LSM 510 confocal laser-scanning microscope (Carl Zeiss) equipped with ×63 oil-immersion objective. Image processing was done with Adobe Photoshop C2 (Adobe Sysytem Inc., San Jose, USA). To perform quantitative image analysis, 10–15 randomly chosen fields that included 8–10 cells each were scanned, using the same setting parameters (i.e. pinhole, laser power, offset gain and detector amplification) below pixel saturation. The mean intensity per cell was determined using the histogram function in the Zeiss LSM 510 Software (version 3.2), and all of the pixel values above background levels were quantified. All of the experiments were repeated at least three times, and representative images are shown. Quantification of number and the size of LAMP1, LAMP2 and cathepsin D positive vesicles were performed using the AnalySIS software (Soft Imaging Systems GmbH, Muenster, Germany). Quantification was carried out on at least 20 cells per condition from two to four independent experiments.

Albumin endocytic uptake

The endocytosis assay was performed as described previously (22). Monolayers of PT cells were washed with warm Hank's balanced salt solution (HBSS without phenol red with 10 mM glucose, 5 mM glycine, 1 mM alanine, 15 mM HEPES, final pH to 7.40 with TRIS base and osmolality to 325 mOsm/kg with mannitol) after which they were incubated with 0.5 mg/ml FITC- BSA for 15 min at 37°C. After the incubation, primary cultures were washed 6 times with cold HBSS (4°C) and lysed in lysis buffer (1 mM EDTA, 20 mM imidazole pH 7.2 and 250 mM sucrose). The fluorescence in the lysate was measured in a single-beam fluorimeter (PerkinElmer, Santa Clara, USA) at an excitation wavelength of 490 ± 10 nm and emission

wavelength at 520 ± 10 nm. Fluorescence was normalized for the amount of proteins in the primary cell cultures measured using the bicinchoninic acid protein assay (Pierce, Aalst, Belgium).

For live-cell imaging, confluent monolayers of mPTC were incubated with 0.5 mg/ml FITC-conjugated BSA for 7 min at 37°C and washed. Fluorescence was chased up to 45 min after exposure of the cells to albumin. Cells were examined using the Zeiss LSM510Meta Confocal microscope (Carl Zeiss, Belgium).

Quantification of lysosome distribution

To score lysosome distribution, cells were categorized into perinuclear-dominant lysosomal pattern (more than 50% of LAMP1-positive vesicles localized in the perinuclear region) and peripheral-dominant pattern (more than 50% of the vesicles localized in the peripheral region). Quantification was based on at least three independent experiments, each carried out in triplicate, and 100 cells were counted in each slide; the scorer was blinded to treatment. The data are expressed as a proportion of cells with predominantly ($>50\%$) perinuclear lysosomes.

FRAP assay for cathepsin B activity

The lysosomal cathepsin B activity was measured in primary cultures of PT cells using the membrane-permeable Magic Red[TM] tracer coupled to the FRAP assay. The primary cells were transferred to a physiological imaging buffer (NaCl 130 mM, KCl 5 mM, CaCl$_2$ 2.5 mM, MgCl$_2$ 2.5 mM, HEPES 25 mM) containing the Magic Red cathepsin B peptide (AbD Serotec, Oxford, UK) added to the medium at 1:10 dilution and incubated at 37°C. Live cell imaging and fluorescence recovery analysis were done using LSM510 Zeiss confocal microscope. To achieve photobleaching of individual Magic Red-positive lysosomes, areas of interest were drawn around selected spots, and movie acquisition was started. Sixty seconds later, the spots were photobleached using 458, 488, 543, and 633 nm lasers with a $63\times$ objective. Approximately 5 to 8 cells per field of view were bleached for a duration of 100 bleaching cycles according to the bleaching module within LSM510 software (LSM 510 version 3.2). The recovery of fluorescence was monitored over time (400 s) by scanning the bleached area at the conventional (low) laser power to minimize photobleaching during sampling. To analyze the rate of recovery, we compared the fluorescence of the photobleached area to that of an adjacent unbleached area of the same cell with similar fluorescence intensity. For each time point, the fluorescence of the bleached area was normalized to that of corresponding control (unbleached) area to correct for possible drift of the focal plane or photobleaching incurred during the low light sampling. Quantification of fluorescence was carried out using Volocity software, with each data set having approximately 25 cells in each condition analyzed, and each curve representing results from 3 experiments. For each experimental FRAP curve, the $\tau_{1/2}$ value was calculated by fitting the data with Boltzmann function. The FRAP experiments were performed at 37°C on Zeiss LSM510 microscope equipped with Zeiss confocal scanning laser using a x63 1.4 numerical aperture objective. The specificity of tracer was verified by incubating primary cultured cells with 100 μM leupeptin (Calbiochem, Merck Millipore, Billerica, USA) dissolved in dimethyl sulfoxide (DMSO) (vehicle) for 9 h before exposing them to Magic Red (31).

Cystine measurement

The cystine assay was performed as previously described (32). Briefly, dissected tissues or primary cultured cells were homogenized and lysed in the presence of *N*-ethylmaleide to avoid interference from cysteine. Protein was determined on the pellet using the Lowry method (32). After deproteinization, addition of stable isotope d6 cystine and butylation, cystine was measured by liquid chromatography-tandem mass spectrometry using an API 3000 mass spectrometer (Applied Biosystems).

Cell proliferation

Primary cultures of PT cells were incubated at Days 1, 3, 5, 6, 7 and 8 with BrdU (BrdU Cell Proliferation ELISA Kit, Abcam) for 24 h at 37°C. The cells were then fixed and permeabilized, and DNA was denatured. The detector anti-BrdU monoclonal antibody was added for 1 h and then washed away. A secondary horseradish peroxidase-conjugated goat anti-mouse antibody was added, which catalyzed the conversion of the chromogenic substrate, and the coloured reaction product was quantified using a Benchmark Plus microplate spectrophotometer (Bio-Rad).

Statistical analysis

Data were expressed as mean $\pm$ SEM. Significance of differences was assessed by unpaired Student's *t* test. $P < 0.05$ was considered statistically significant.

REFERENCES

1. Avner, E., Harmon, W., Niaudet, P. and Yoshikawa, N. (2009) Pediatric nephrology. In: Igarashi, T. (ed), *Fanconi Syndrome*. Springer-Verlag, Berlin Heidelberg, Germany, pp. 1039–1067.
2. Gahl, W.A., Thoene, J.G. and Schneider, J.A. (2002) Cystinosis. *N. Engl. J. Med.*, **347**, 111–121.
3. Town, M., Jean, G., Cherqui, S., Attard, M., Forestier, L., Whitmore, S.A., Callen, D.F., Gribouval, O., Broyer, M., Bates, G.P. *et al.* (1998) A novel gene encoding an integral membrane protein is mutated in nephropathic cystinosis. *Nat. Genet.*, **18**, 319–324.
4. Cherqui, S., Sevin, C., Hamard, G., Kalatzis, V., Sich, M., Pequignot, M.O., Gogat, K., Abitbol, M., Broyer, M., Gubler, M.C. *et al.* (2002) Intralysosomal cystine accumulation in mice lacking cystinosin, the protein defective in cystinosis. *Mol. Cell. Biol.*, **22**, 7622–7632.
5. Wilmer, M.J., Emma, F. and Levtchenko, E.N. (2010) The pathogenesis of cystinosis: mechanisms beyond cystine accumulation. *Am. J. Physiol. Renal Physiol.*, **299**, F905–F916.
6. Wilmer, M.J., Kluijtmans, L.A., van der Velden, T.J., Willems, P.H., Scheffer, P.G., Masereeuw, R., Monnens, L.A., van den Heuvel, L.P. and Levtchenko, E.N. (2011) Cysteamine restores glutathione redox status in cultured cystinotic proximal tubular epithelial cells. *Biochim. Biophys. Acta*, **1812**, 643–651.
7. Sansanwal, P., Yen, B., Gahl, W.A., Ma, Y., Ying, L., Wong, L.J. and Sarwal, M.M. (2010) Mitochondrial autophagy promotes cellular injury in nephropathic cystinosis. *J. Am. Soc. Nephrol.*, **21**, 272–283.
8. Wilmer, M.J., Christensen, E.I., van den Heuvel, L.P., Monnens, L.A. and Levtchenko, E.N. (2008) Urinary protein excretion pattern and renal expression of megalin and cubilin in nephropathic cystinosis. *Am. J. Kidney Dis.*, **51**, 893–903.
9. Cherqui, S. (2012) Cysteamine therapy: a treatment for cystinosis, not a cure. *Kidney Int.*, **81**, 127–129.
10. Nevo, N., Chol, M., Bailleux, A., Kalatzis, V., Morisset, L., Devuyst, O., Gubler, M.C. and Antignac, C. (2010) Renal phenotype of the cystinosis mouse model is dependent upon genetic background. *Nephrol. Dial. Transplant.*, **25**, 1059–1066.
11. Terryn, S., Jouret, F., Vandenabeele, F., Smolders, I., Moreels, M., Devuyst, O., Steels, P. and Van Kerkhove, E. (2007) A primary culture of mouse proximal tubular cells, established on collagen-coated membranes. *Am. J. Physiol. Renal Physiol.*, **293**, F476–F485.
12. Christ, A., Terryn, S., Schmidt, V., Christensen, E.I., Huska, M.R., Andrade-Navarro, M.A., Hübner, N., Devuyst, O., Hammes, A. and Willnow, T.E. (2010) The soluble intracellular domain of megalin does not affect renal proximal tubular function in vivo. *Kidney Int.*, **78**, 473–474.
13. Gailly, P., Jouret, F., Martin, D., Debaix, H., Parreira, K.S., Nishita, T., Blanchard, A., Antignac, C., Willnow, T.E., Courtoy, P.J. *et al.* (2008) Type III carbonic anhydrase: a novel renal isoform that plays a role in proximal tubule dysfunction. *Kidney Int.*, **74**, 52–61.
14. Lima, W.R., Parreira, K.S., Devuyst, O., Caplanusi, A., N'kuli, F., Marien, B., Van Der Smissen, P., Alves, P.M., Verroust, P., Christensen, E.I. *et al.* (2010) ZONAB promotes proliferation and represses differentiation of proximal tubule epithelial cells. *J. Am. Soc. Nephrol.*, **21**, 478–488.
15. Fraldi, A., Annunziata, F., Lombardi, A., Kaiser, H.J., Medina, D.L., Spampanato, C., Fedele, A.O., Polishchuk, R., Sorrentino, N.C., Simons, K. *et al.* (2010) Lysosomal fusion and SNARE function are impaired by cholesterol accumulation in lysosomal storage disorders. *EMBO J.*, **29**, 3607–3620.
16. Settembre, C., Fraldi, A., Medina, D.L. and Ballabio, A. (2013) Signals from the lysosome: a control centre for cellular clearance and energy metabolism. *Nat. Rev. Mol. Cell. Biol.*, **14**, 283–296.
17. Christensen, E.I., Verroust, P.J. and Nielsen, R. (2009) Receptor mediated endocytosis in renal proximal tubules. *Pflugers Arch.*, **458**, 1039–1048.
18. Devuyst, O. and Pirson, Y. (2007) Genetics of hypercalciuric stone forming diseases. *Kidney Int.*, **72**, 1065–1072.
19. Devuyst, O. and Thakker, R.V. (2010) Dent's disease. *Orphanet J Rare Dis.*, **5**, 28.
20. Kantarci, S., Al-Gazali, L., Hill, R.S., Donnai, D., Black, G.C., Bieth, E., Chassaing, N., Lacombe, D., Devriendt, K., Teebi, A. *et al.* (2007) Mutations in LRP2, which encodes the multiligand receptor megalin, cause Donnai-Barrow and facio-oculo-acoustico-renal syndromes. *Nat Genet.*, **39**, 957–959.
21. Fyfe, J.C., Madsen, M., Højrup, P., Christensen, E.I., Tanner, S.M., de la Chapelle, A., He, Q. and Moestrup, S.K. (2004) The functional cobalamin (vitamin B12)-intrinsic factor receptor is a novel complex of cubilin and amnionless. *Blood*, **103**, 1573–1579.
22. Reed, A.A., Loh, N.Y., Terryn, S., Lippiat, J.D., Partridge, C., Galvanovskis, J., Williams, S.E., Jouret, F., Wu, F.T., Courtoy, P.J. *et al.* (2010) CLC-5 and KIF3B interact to facilitate CLC-5 plasma membrane expression, endocytosis, and microtubular transport: relevance to pathophysiology of Dent's disease. *Am. J. Physiol. Renal. Physiol.*, **298**, F365–F380.
23. Nielsen, R., Courtoy, P.J., Jacobsen, C., Dom, G., Lima, W.R., Jadot, M., Willnow, T.E., Devuyst, O. and Christensen, E.I. (2007) Endocytosis provides a major alternative pathway for lysosomal biogenesis in kidney proximal tubular cells. *Proc. Natl. Acad. Sci. U S A.*, **104**, 5407–5412.
24. Christensen, E.I., Devuyst, O., Dom, G., Nielsen, R., Van der Smissen, P., Verroust, P., Leruth, M., Guggino, W.B. and Courtoy, P.J. (2003) Loss of chloride channel ClC-5 impairs endocytosis by defective trafficking of megalin and cubilin in kidney proximal tubules. *Proc. Natl. Acad. Sci. USA*, **100**, 8472–8477.
25. Jouret, F., Walrand, S., Parreira, K.S., Courtoy, P.J., Pauwels, S., Devuyst, O. and Jamar, F. (2010) Single photon emission-computed tomography (SPECT) for functional investigation of the proximal tubule in conscious mice. *Am. J. Physiol. Renal. Physiol.*, **298**, F454–F460.
26. Tanaka, K., Terryn, S., Geffers, L., Garbay, S., Pontoglio, M. and Devuyst, O. (2010) The transcription factor HNF1α regulates expression of chloride-proton exchanger ClC-5 in the renal proximal tubule. *Am. J. Physiol. Renal Physiol.*, **299**, F1339–F1347.
27. Hallman, M.A., Zhuang, S. and Schnellmann, R.G. (2008) Regulation of dedifferentiation and redifferentiation in renal proximal tubular cells by the epidermal growth factor receptor. *J. Pharmacol. Exp. Ther.*, **325**, 520–528.
28. Wang, S.S., Devuyst, O., Courtoy, P.J., Wang, X.T., Wang, H., Wang, Y., Thakker, R.V., Guggino, S. and Guggino, W.B. (2000) Mice lacking renal chloride channel, CLC-5, are a model for Dent's disease, a nephrolithiasis disorder associated with defective receptor-mediated endocytosis. *Hum. Mol. Genet.*, **9**, 2937–2945.
29. Jouret, F., Bernard, A., Hermans, C., Dom, G., Terryn, S., Leal, T., Lebecque, P., Cassiman, J.J., Scholte, B.J., de Jonge, H.R. *et al.* (2007) Cystic fibrosis is associated with a defect in apical receptor-mediated endocytosis in mouse and human kidney. *J. Am. Soc. Nephrol.*, **18**, 707–718.
30. Bustin, S.A., Benes, V., Garson, J.A., Hellemans, J., Huggett, J., Kubista, M., Mueller, R., Nolan, T., Pfaffl, M.W., Shipley, G.L. *et al.* (2009) The MIQE guidelines: minimum information for publication of quantitative real-time PCR experiments. *Clin. Chem.*, **55**, 611–622.
31. Orenstein, S.J., Kuo, S.H., Tasset, I., Arias, E., Koga, H., Fernandez-Carasa, I., Cortes, E., Honig, L.S., Dauer, W., Consiglio, A. *et al.* (2013) Interplay of LRRK2 with chaperone-mediated autophagy. *Nat. Neurosci.*, **16**, 394–406.
32. Chabli, A., Aupetit, J., Raehm, M., Ricquier, D. and Chadefaux-Vekemans, B. (2007) Measurement of cystine in granulocytes using liquid chromatography-tandem mass spectrometry. *Clin. Biochem.*, **40**, 692–698.